Enhanced CO_2 conversion by frosted dielectric surface with ZrO_2 coating in a dielectric barrier discharge reactor

Wanyan Ding,[1] Mengyu Xia,[1] Chenyang Shen,[1] Yaolin Wang[2], Zhitao Zhang,[1] Xin Tu,[2]*

Chang-jun Liu[1]*

1. School of Chemical Engineering and Technology, Tianjin University, Tianjin 300072, China

2. Department of Electrical Engineering and Electronics, University of Liverpool, Liverpool L69 3GJ, UK

*Corresponding authors. Emails: xin.tu@liverpool.ac.uk (Xin Tu) and cjL@tju.edu.cn (Chang-jun Liu)

ABSTRACT

The direct conversion of CO_2 into CO and O_2 by dielectric barrier discharge (DBD) non-thermal plasma is effective with simple setup, easy on/off operation and flexibility to the CO_2 source. Herein, we demonstrated the frosted dielectric surface without and with ZrO_2 coating can significantly improve the conversion and energy efficiency of the plasma CO_2 decomposition in a DBD reactor, compared to the conventional un-frosted dielectric surface without ZrO_2 coating. The use of the frosted dielectric surface increases the dielectric capacitance, mean electron energy and micro-discharge channels, leading to increased CO_2 conversion and energy efficiency. The coating of ZrO_2 of a high dielectric constant further improves the discharge performances with further increased CO_2 conversion and energy efficiency. The highest energy efficiency of 7.7% was achieved within the tested conditions. The effect of CO_2 adsorption on ZrO_2 coating is negligible because of the low coating amount.

Keywords: Dielectric barrier discharge; Non-thermal plasma; CO_2 conversion; Frosted dielectric surface; ZrO_2

1. Introduction

The capture and utilization of carbon dioxide has drawn significant attention worldwide [1-2]. CO_2 is a linear inert molecule with a double bond between the carbon and oxygen atoms (O=C=O), which requires a minimum energy of 5.5 eV to break (reaction (1)) [3-4].

$$CO_2 \rightarrow \frac{1}{2}O_2 + CO \qquad (\Delta H) = 280 \text{ kJ/mol} \qquad (1)$$

Among various methods exploited for CO_2 conversion, the CO_2 decomposition via cold plasmas is promising with the rapid progress in renewable energies [5-7]. Plasma is defined as the fourth state of matter. It is very different from the conventional three states (solid, liquid, and gas). It is usually formed by partial (or complete) ionization/dissociation of gas molecules under energetic excitation [8-9]. Plasma is thus a collection of molecules, free radicals, excited species, ions, photons and electrons [10]. Cold plasma or non-thermal plasma is a kind of plasma phenomenon. It can be initiated at ambient conditions and operated at temperatures ranging from room temperature to several hundred Kelvin. The average electron temperature in cold plasmas is typically 10000-100000 K (1-10 eV), while its gas temperature can remain as low as room temperature [5,11]. Obviously, this kind of non-thermal distribution of energy is very useful for the activation of inert molecules like CO_2 [12]. Increasing publications can be found in the literature on plasma CO_2 decomposition [4,13-27]. Among various cold plasmas exploited, dielectric barrier discharge (DBD) is unique [4,13,16,20,26-27] because of its high effectiveness, simple setup, convenient monitoring, flexibility for scale-up, and easy on/off operation [28]. Moreover, the physical properties of the dielectric barrier can affect the characteristics of DBD plasma by tuning the density of discharges [7]. Even large-scale ozone production, surface treatment and others have been industrialized considering its simplicity [29].

At present, some researchers have evaluated the CO_2 decomposition reaction using DBD plasma reactors. Mei *et al*. [13] studied the effect of the operating parameters (discharge frequency, carbon dioxide flow rate, discharge length, discharge power, discharge gap and dielectric material thickness) on CO_2 conversion in a cylindrical DBD reactor. The results showed the feed flow rate and discharge power are the key parameters that determine CO_2 decomposition. The latter has a more significant effect on energy efficiency. Xu *et al*. [30] pointed out that diluting CO_2 with Ar/N_2 can increase the conversion of CO_2, but is accompanied by the formation of by-products (O_3/N_2O, NO, NO_2). Ramakers *et al*. [31] also showed that the effect of Ar on the DBD plasma CO_2 conversion is more pronounced than that of He. In addition, a hybrid plasma system containing packing materials/catalysts can partially compensate for the shortcomings of low conversion of CO_2 in DBD plasma reactors. Taghvaei *et al*. [32] coated different packing materials ($BaTiO_3$, TiO_2, CeO_2, ZrO_2, CaO, Al_2O_3, Fe_3O_4, and SiO_2) on three-dimensional polyurethane foams and incorporated them into the discharge zone of a DBD reactor. They proved the coating of metal oxides boosts the conversion proportional to their dielectric constant. In addition, Ray *et al*. [33] reported that placing 15% MO/γ-Al_2O_3 (M=Ni and Cu) catalysts into the discharge zone enhanced the CO_2 conversion by 42% and 112%, respectively, compared with the plasma CO_2 decomposition without a catalyst, thus demonstrating the importance of catalysts in the plasma-assisted CO_2 conversion. However, these filling materials will reduce the reaction space and gas residence time in the plasma zone, and even affect discharge characteristics [6]. It is well recognized that the modification of the DBD reactor provides a new solution to enhance CO_2 conversion. However, most of the reported research focused on the design of internal and external electrodes [26,34,35]. Less

attention has been paid to the tuning of dielectric materials to enhance the reaction performance of the plasma CO_2 decomposition.

In this work, we report the improvement of the micro-discharge performance of DBD for enhanced CO_2 conversion by using the ZrO_2-coated frosted quartz tube as the dielectric material. The improvement mechanism by the frosted dielectric surface and the ZrO_2 coating was investigated.

2. Experimental

2.1. Experimental setup

Fig. 1 shows the schematic diagram of the experimental setup. A cylindrical DBD reactor with a double dielectric was employed in this work. As shown in Fig. 2, a 316L stainless steel round rod with a diameter of 3 mm was used as the high-voltage internal electrode, which was located on the axis of the tubular reactor and connected to the plasma source. A quartz tube covering the electrode with an inner diameter of 3 mm and a wall thickness of 1 mm was served as a dielectric barrier. The outer surface of the reactor was tightly covered with an 80 mm wide aluminium foil layer, which was used as the ground electrode. The reactor had a fixed discharge length. For the preparation of the oxide-coated tube, the frosted quartz tube prepared by sandblasting process was used to ensure the uniformity of ZrO_2 coating. The digital photos of the three types of dielectric barrier surfaces are shown in Fig. 3. The DBD reactor was connected to a plasma power supply (CTP-2000K, Nanjing Suman Plasma Technology Co., Ltd) with a maximum peak voltage of 30 kV and a discharge frequency of 5-20 kHz. A 1000:1 voltage probe (PHV4-8596, LeCroy PPE) was used to measure the applied voltage, and an external capacitor (0.47 μF) and a resistor (50 Ω) were connected in series between the DBD

reactor and the ground wire to measure the transferred charge and current during the discharge process. All electrical signals were recorded by a digital oscilloscope (DSO6052A, Agilent Technologies). Because the use of any co-feed gas, including argon or helium, will increase the CO_2 conversion, pure CO_2 was used here as the feed gas, to study the intrinsic behavior of the plasma CO_2 conversion. The feed rate was controlled by a mass flow controller (MFC, D07-7, Beijing SevenStar Flow Co., Ltd). Because the carbon dioxide decomposition is not an iso-volumetric reaction, a soap film flowmeter was used to measure the effluent from the reactor for the calculation of CO_2 conversion.

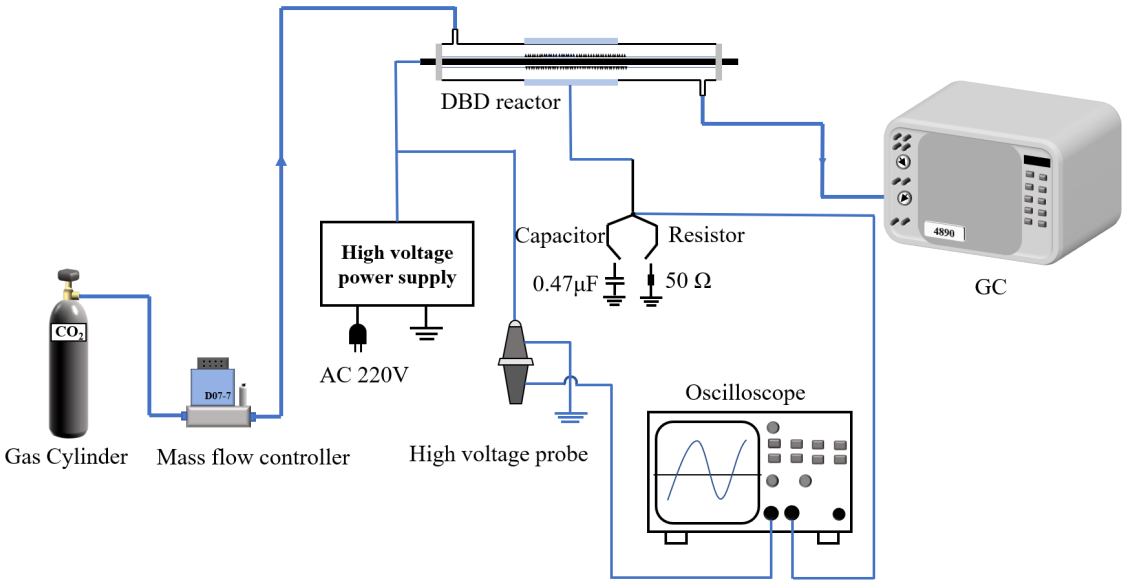

Fig. 1. Schematic of the experimental setup.

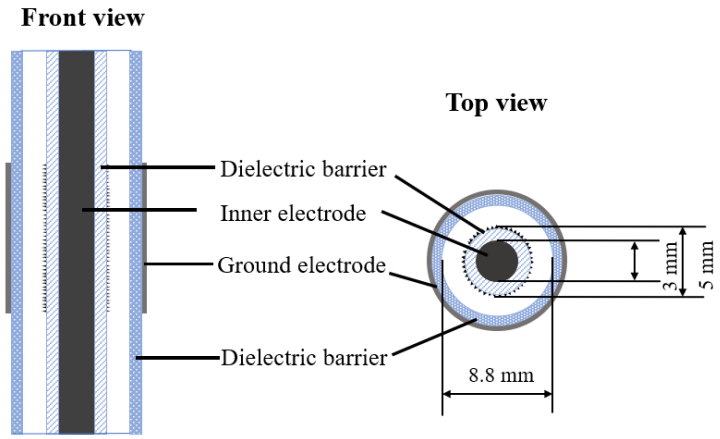

Fig. 2. DBD reactor with a frosted dielectric barrier.

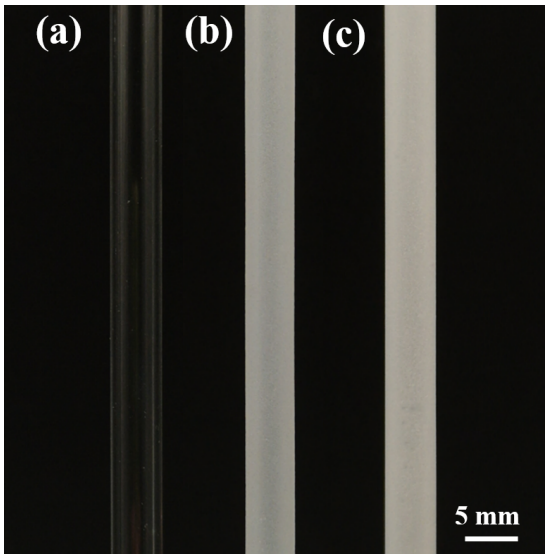

Fig. 3. Digital photos of quartz tubes with different surfaces: (a) un-frosted surface; (b) frosted surface; (c) frosted surface with ZrO_2 coating.

2.2 Gas analysis

The gas composition after the reaction was detected by a gas chromatograph (GC, Agilent 4890D) equipped with a thermal conductivity detector (TCD) and a flame ionization detector (FID). A six-way valve system was used for online sampling. The main products of CO_2

decomposition were CO and O_2, which were quantitatively analyzed by the external standard method.

The conversion of CO_2 (X), specific energy input (SEI) and energy efficiency of the plasma process (η) are determined by:

$$X_{CO_2}(\%) = \frac{CO_2 \text{ converted}(\text{mol s}^{-1})}{CO_2 \text{ introduced}(\text{mol s}^{-1})} \times 100\% \quad (2)$$

$$\text{SEI}\left(\text{kJ L}^{-1}\right) = \frac{\text{Discharge power (W)}}{CO_2 \text{ flow rate}(\text{ml s}^{-1})} \quad (3)$$

$$\eta\ (\%) = \frac{CO_2 \text{ flow rate}(\text{ml s}^{-1}) \times X_{CO_2}(\%) \times \Delta H\left(\text{kJ mol}^{-1}\right)}{22.4 \times \text{Discharge power (W)}} \quad (4)$$

where ΔH is the standard reaction enthalpy of pure CO_2 decomposition, and the value is 280 kJ mol^{-1} [4,13]. The discharge power is calculated via the Q-U Lissajous figure, while the gas flow rate can be controlled directly via the mass flow controller.

2.3 Characteristics of the DBDs

To investigate the effects of ZrO_2 coating and the frosted surface on the electric properties of DBDs, it is usually assumed that the DBD reactor can be simplified and equivalent to a circuit composed of the equivalent dielectric capacitance (C_d) in the dielectric barrier layer and the equivalent gap capacitance (C_g) in the gas discharge gap in series (Fig. S1(a)) [36-38]. The analysis of the Lissajous figure, shown in Fig. S1(b), is a common method for the characterization of DBDs [34,38-40]. Based on this analysis, the mean electron energy and the electron energy distribution function (EEDF) can be calculated with the Boltzmann equation by Boltzmann solver BOLSIG+ [41]. The details of the calculation have been given in our previous work [40].

2.4 ZrO_2 coating over the dielectric barrier surface

To load ZrO_2 on the dielectric barrier surface, the quartz was firstly frosted, as shown in Fig. S2. A zirconium nitrate solution with a concentration of 1 mol/L was prepared by adding 8.5852 g of zirconium nitrate ($Zr(NO_3)_4 \cdot 5H_2O$, Tianjin Kemiou Chemical Reagent, China) to a 20 ml deionized water. The obtained mixture was heated and stirred at 60 °C for 10 min in a magnetic heater agitator. Next, a dropper was used to drip the precursor solution onto the frosted quartz tube until the frosted surface was completely wet. To prevent local accumulation, the excess precursor solution on the surface was removed by rotating back and forth. Following that, the prepared tube was dried in the oven for 12 h. Finally, the dielectric surface coated with ZrO_2 was obtained by calcining the dried tube in a furnace at 500 °C for 3 h. With the ZrO_2 coating, the discharge gap is ca. 1.9 mm.

2.5 Characterization of dielectric barrier surface

The surface roughness and micro-morphology of the quartz tubes were characterized by an atomic force microscope (AFM, Multimode V). The test side of the sample was placed upwards and pasted on a mica sheet. The scan size was 20 μm × 20 μm at a scan rate of 0.5 Hz.

The optical microscope images of the quartz tubes were taken by the OLYMPUS SZ61 optical microscope (OM). A uniform and bright field of the view was obtained by adjusting a suitable light source.

The surface morphology and element mapping of the tube coated with ZrO_2 were scanned by the field emission scanning electron microscope (SEM, Regulus 8100). A small piece of quartz tube sample was taken. The side without ZrO_2 was stuck to the conductive glue before measurement.

3 Results and discussions

3.1 Analysis of dielectric barrier surface roughness

In this experiment, to evaluate the influence of dielectric surface roughness on the plasma conversion of CO_2, abrasive papers with different mesh numbers (i.e., 2000 mesh, 800 mesh, 400 mesh, and 240 mesh) were used to roughen the dielectric surfaces to different levels. Note smaller mesh number gives greater roughness to the dielectric surface. Fig. S3 shows digital photos of dielectric surfaces after roughening. The surface roughness parameter Ra was measured by AFM. The three-dimensional topographies of the surfaces measured by AFM are shown in Fig. 4. Clearly, the roughened surfaces have more or less defects, and the specific gully depths are shown in Table 1.

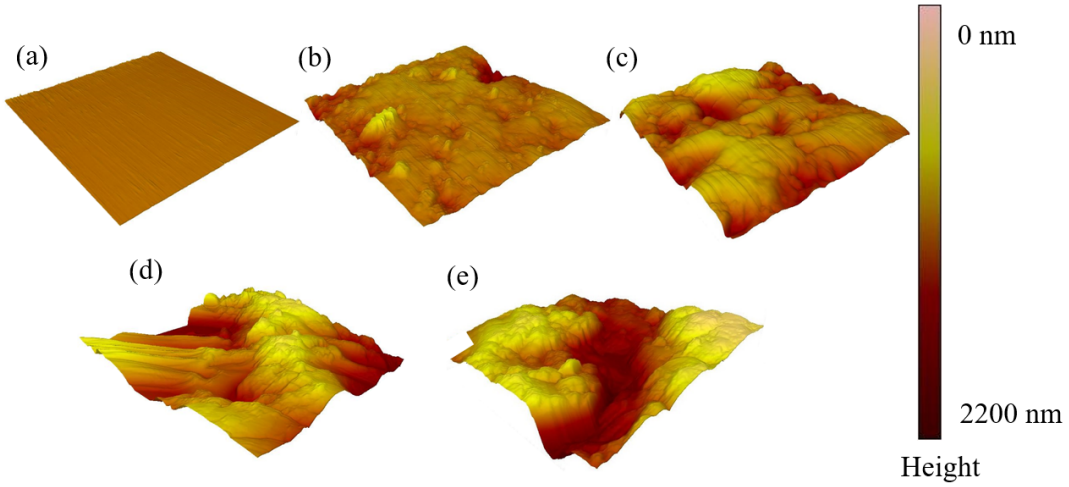

Fig. 4. Three-dimensional topographies of the dielectric barrier surfaces after roughing with different meshes of abrasive papers: (a) un-frosted; (b) 2000 mesh; (c) 800 mesh; (d) 400 mesh; (e) 240 mesh (scan size: 20 μm × 20 μm).

Table 1. Data measured by AFM

		Mesh number of abrasive paper			
	Un-frosted tube	2000	800	400	240
Ra (nm)	9	118	195	369	632
Gully depth (nm)	175.1	581.8	626.9	1093.1	1992.6

3.2 Analysis of ZrO_2 coated tube

Here, to evaluate the uniformity of the coating material on the dielectric barrier surface, the quartz tube was analyzed by OM, SEM and EDX mapping. As shown in Fig. 5(a), the coated quartz tube is milky white, and the coated ZrO_2 dielectric layer has been integrated with the frosted surface as a whole. The SEM images (Fig. 6) show that the structure does not change noticeably when exposed to plasma discharge. Elemental mapping analysis (Fig. 5(b)) also confirms the result, indicating that ZrO_2 is uniformly distributed on the frosted dielectric barrier. Because of the low loading of ZrO_2 on the tube in this work, the CO_2 adsorption on ZrO_2 can be negligible.

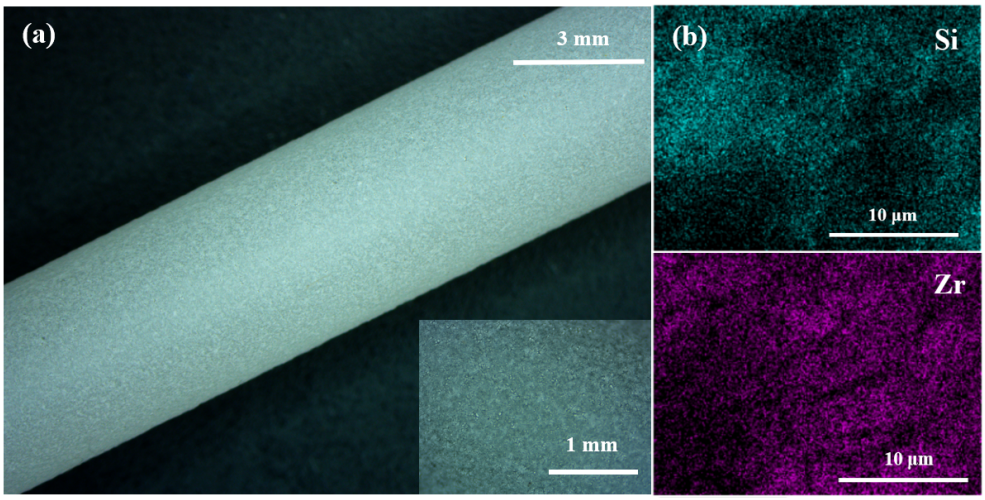

Fig. 5. (a) Optical microscope images and (b) elemental mapping analysis for a ZrO_2

coated dielectric barrier.

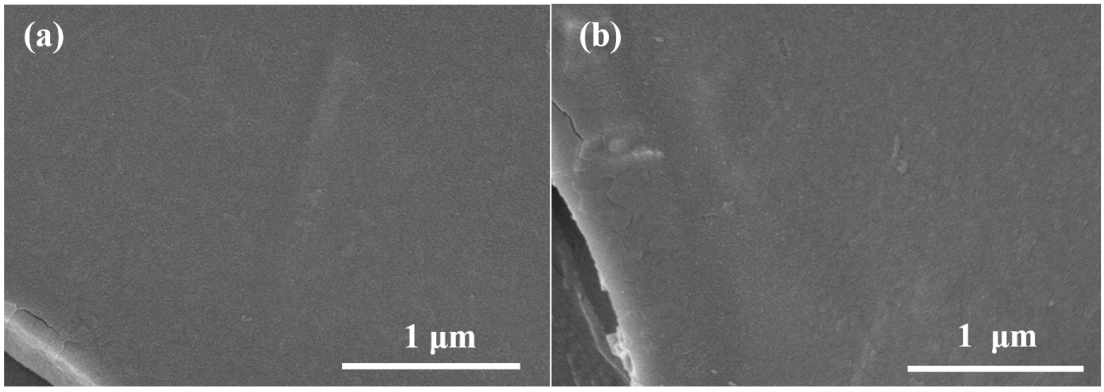

Fig. 6. SEM images of ZrO_2 coated dielectric surface (a) before and (b) after exposure to plasma discharge.

3.3 Effect of frosted dielectric barrier surface on the plasma CO_2 decomposition

Fig. 7 shows the conversion of CO_2 increases gradually when increasing the roughness of the dielectric surface. The highest CO_2 conversion of 11.7% is achieved when the roughness of the dielectric surface is 632 nm, 31.5% higher than that over the un-frosted dielectric surface (Ra = 9 nm).

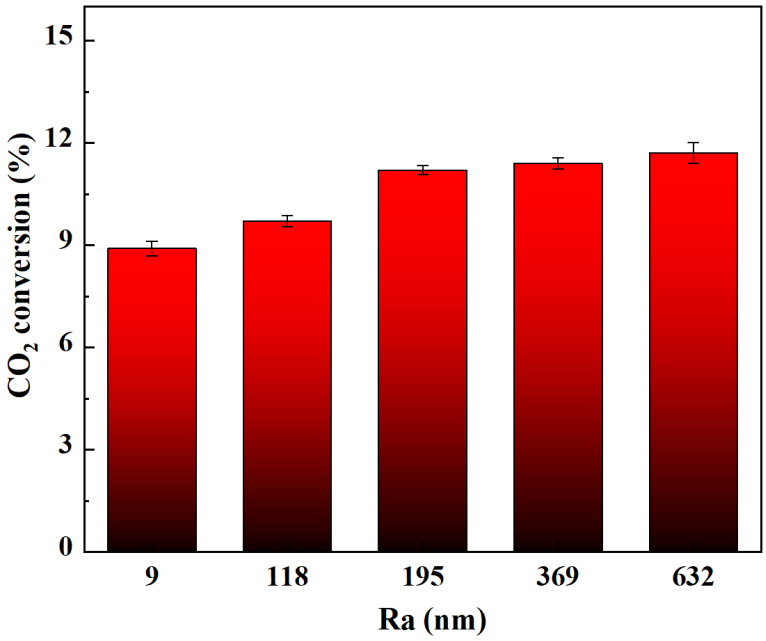

Fig. 7. Effect of dielectric barrier roughness (Ra) on CO_2 conversion. (SEI=29 kJ/L; total flow rate: 30 mL/min; frequency: 8.8 kHz)

In general, the electric field can be enhanced by roughness or geometric distortion [42,43]. Due to the difference in the depth of the dielectric surface defects, the surface charge adsorption and desorption capabilities are significantly changed, which leads to different charge densities accumulated on the dielectric surface. A large amount of charge local accumulation centers is thus formed. This causes more discharge channels, resulting in a higher conversion of CO_2. From the experimental results, the dielectric surface with a roughness of 632 nm corresponding to the use of 240 mesh abrasive paper is most significantly affected by this mechanism.

3.4 Effect of ZrO_2 coating on the plasma CO_2 decomposition

Fig. 8 shows the effect of ZrO_2 coating and gas flow rate on the plasma CO_2 decomposition. The ZrO_2 coating on the frosted dielectric surface leads to a further remarkably increase in the conversion of CO_2, compared to the un-coated frosted dielectric surface. In the entire flow rate range, the CO_2 conversion and energy efficiency over the ZrO_2 coated dielectric barrier surface are higher than those with the un-frosted dielectric and frosted dielectrics. The highest CO_2 conversion is 21.7% over the ZrO_2 coated dielectric barrier at a gas flow rate of 10 ml/min, while the conversion of CO_2 drops to 16.3% and 13.2% on the frosted and the un-frosted dielectric surface, respectively, at the same CO_2 gas flow rate. On the other hand, the energy efficiency increases with the increasing CO_2 flow rate. The ZrO_2 coating significantly enhances the energy efficiency. There exists a trade-off between the conversion and energy efficiency.

The highest energy efficiency is 7.7% at the gas flow rate of 50 ml/min. The energy efficiency can be increased when further increasing the gas flow rate.

Fig. S4 presents a stability test result. Because DBD plasma reaction has the advantage of easy on/off operation, the study through cyclic test is used to prevent the excessive thermal effect of DBD plasma reaction caused by the discharge reaction. Each cycle lasts for 30 min, and the reaction will restart each time when the plasma reactor is cooled down to room temperature through the flowing feed gas. From the results, excellent stability can be observed when a frosted dielectric or ZrO_2 coated dielectric is used.

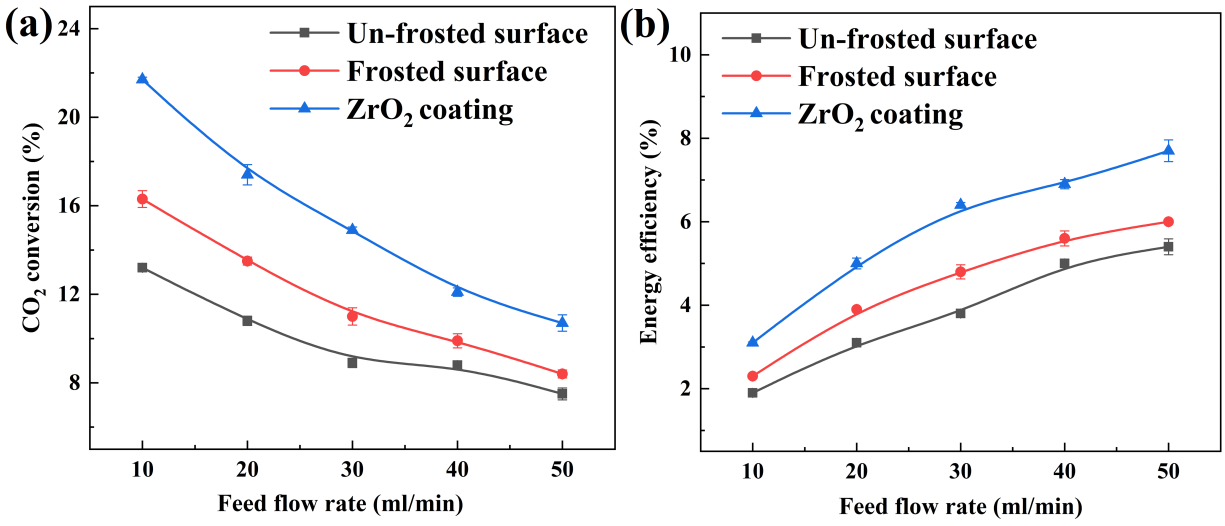

Fig. 8. Effect of feed flow rate on CO_2 conversion and energy efficiency with different types of dielectric surfaces (discharge power: 14.5 W; discharge length: 80 mm; frequency: 8.8 kHz; discharge gap: 0.19 cm; the maximum discharge voltage: 11.8 kV (un-frosted surface), 11.6 kV (frosted surface), 11.0 kV (ZrO_2 coated surface)).

Fig. 9 shows the effect of frequency on the CO_2 conversion and energy efficiency. As the

frequency increases from 8.8 to 10 kHz, the CO_2 conversion and energy efficiency decrease slightly. This cannot be explained from the perspective of the total number and average lifetime of micro-discharges or discharge currents [44]. It may be due to the discrepancy in the shape of the electron energy distribution function at different frequencies. More electrons, which are good for breaking the C=O bond in CO_2 molecule, will be generated at a lower frequency [29]. CO_2 conversion thus decreases at a higher frequency. In addition, the result obtained in this work is consistent with the work by Zhu *et al*. [27], who put the packing materials in the discharge gap to improve the CO_2 conversion. The relevant maximum discharge voltages are shown in Table S1.

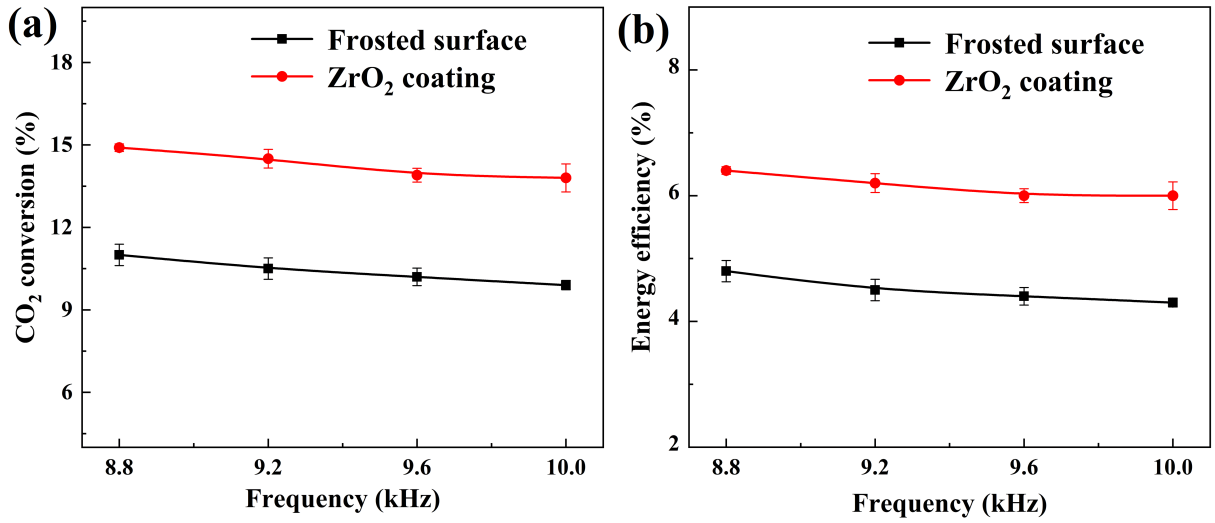

Fig. 9. Effect of discharge frequency on CO_2 conversion and energy efficiency (SEI=29 kJ/L; feed flow rate: 30 ml/min; discharge length: 80 mm; discharge gap: 0.19 cm).

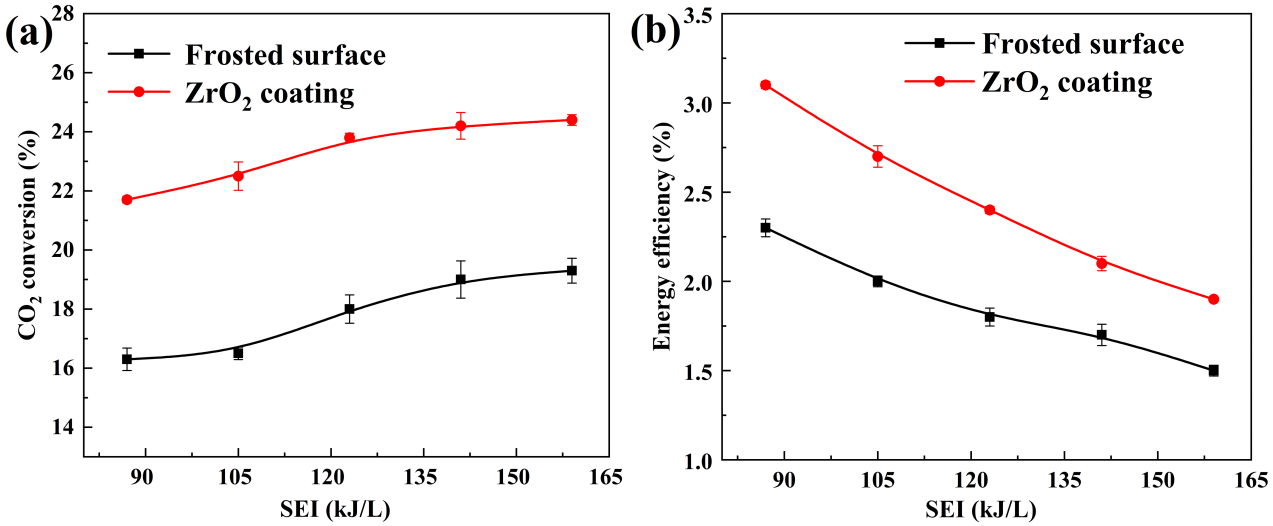

Fig. 10. Effect of discharge power on CO_2 conversion and energy efficiency (feed flow rate: 10 ml/min; discharge length: 80 mm; discharge gap: 0.19 cm; frequency: 8.8 kHz).

SEI is generally regarded as one of the key factors in the CO_2 conversion process. As described in Eq. (3), the SEI value is determined by the gas flow rate and the discharge power. Fig. 8 shows a higher gas flow rate leads to lower CO_2 conversion but high energy efficiency. When other operating parameters are fixed, increasing the CO_2 flow rate would decrease the residence time of CO_2 in the plasma, which reduces the probability of collisions between CO_2 molecules and energetic species (e.g., electrons and reactive species), resulting in the decreased conversion of CO_2. However, the amount of CO_2 excited by the plasma per unit time increases at a higher gas flow rate, while the percentage of energy consumed by the plasma reaction for CO_2 conversion increases, thus the energy efficiency is higher at a higher gas flow rate.

As shown in Fig. 10, the conversion of CO_2 increases as discharge power increases. However, the energy efficiency shows a reverse trend. Specifically, varying the SEI from 87 to 159 kJ/L increases the CO_2 conversion from 16.3% to 19.3% when using the frosted dielectric surface in the DBD reactor. For the ZrO_2 coated dielectric surface, the CO_2 conversion increases

from 21.7% to 24.4% when increasing the SEI from 87 to 159 kJ/L. The amplitude and number of current pulses increase with the increase of the discharge power [26], which induces more high energetic electrons and discharge channels. Therefore, appropriately increasing the discharge power is conducive to CO_2 conversion. However, higher discharge power leads to more energy loss released in the form of heating in the plasma process, which in turn reduces the energy efficiency of the plasma process. A balance between the CO_2 conversion and energy efficiency would be considered for the potential applications.

Table 2 compares the CO_2 conversion and energy efficiency of DBD plasma CO_2 decomposition at atmospheric pressure. From Table 2, the frosted dielectric surface with ZrO_2 coating shows higher energy efficiency, compared to the same reaction without packing materials or catalysts [26,34,45-47]. Considering the difficulty in the loading and removal of particles or powders in the discharge gap (normally 1~3 mm) of the conventional DBD reactor, the frosted dielectric surface with ZrO_2 coating represents a significant advance in the design of more efficient plasma-catalytic reactors for gas conversions not limited to CO_2 decomposition.

Table 2. Comparison of CO_2 conversion and energy efficiency in different specific operation conditions by DBD plasma

Specific operation condition	SEI (kJ/L)	Conversion (%)	Energy efficiency (%)	Ref.
ZrO_2 coating	43.5	17.4	5.0	This work
	17.4	10.7	7.7	
Segmented outer Electrode	53.4	13.1	3.1	[34]
Electrode made of compact copper powder	23.2	9.2	5.0	[26]
NaCl solution as outer Electrode	53.9	15.1	3.5	[45]
Discharge length of 11.2 cm	53	12.6	3.0	[46]
Copper foil as outer electrode	67.5	9.5	1.8	[47]

3.5 Discharge characteristics

According to the previous work by Takuma [48], the electric field can be enhanced with the increase of the dielectric constant of the dielectric material at the contact. While, in the gas discharge, the electric field plays a key role in determining the plasma reaction performance, as it changes the electron energy distribution function. Higher electric field results in higher mean electron energy, which increases the electron impact reaction rate [43,49-50]. Therefore, when the ZrO_2 dielectric material is coated onto the frosted dielectric surface, the dielectric constant rises from ε=3.9 (i.e., SiO_2) to ε=25 (i.e., ZrO_2) [39,42], the rate of CO_2 dissociation will be significantly accelerated. It is worth noting that the unique configuration of ZrO_2 coated frosted

dielectric surface does not change the reactant residence time and discharge gap in the DBD reactor.

Fig. 11(a) plots the discharge current waveforms of the CO_2 DBD. Since a sinusoidal voltage signal is applied to the electrodes of the DBD, each electrode alternatively serves as a cathode and an anode [51]. Therefore, the discharge current waveforms have repeatability with typical filamentary discharge observed. This kind of filamentary discharge or micro-discharge can be regarded as a reaction channel. The more micro-discharges, the more reaction channels are created, which enhance the reactions between highly active species [52].

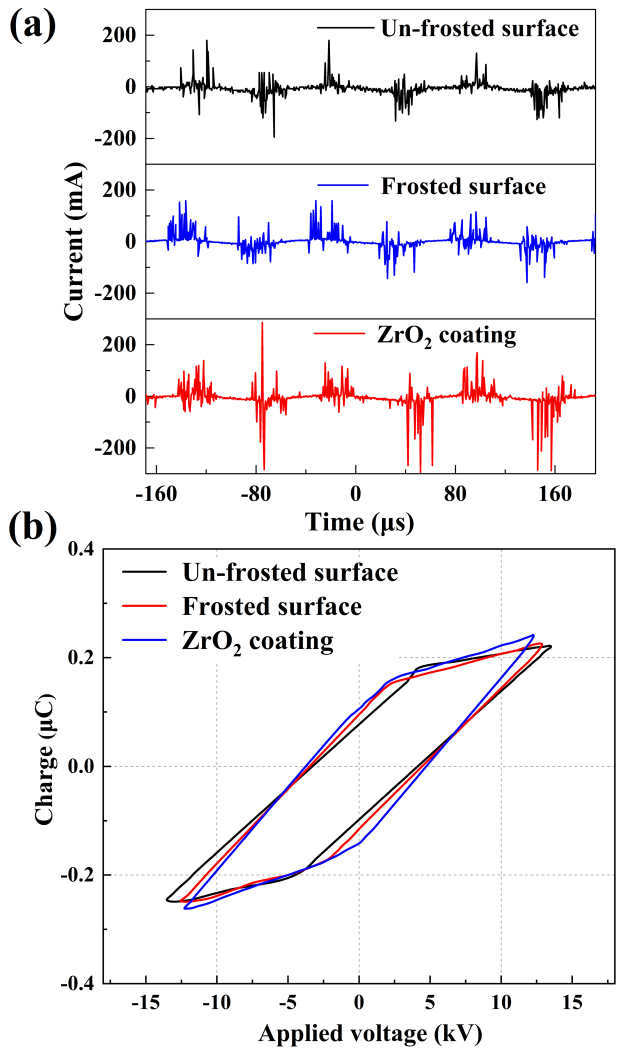

Fig. 11. (a) The current signals and (b) Lissajous figures of the CO_2 DBD with different types of dielectric barriers (discharge power: 26.5 W; frequency: 8.8 kHz).

Table 3. Electrical parameters of CO_2 plasma

Dielectric barrier surface type	Peak applied voltage (kV)	C_d (pF)	Q_{pk-pk}* (μC)	E † (kV cm^{-1})	E/N ‡ (Td)
Un-frosted surface	13.4	24.1±0.1	0.46±0.01	14.7±0.4	78.9
Frosted surface	12.8	26.7±0.9	0.48±0.01	15.8±0.5	84.5
ZrO_2 coating	12.2	31.0±0.3	0.51±0.01	17.4±0.5	93.0

* Q_{pk-pk} means the peak to peak charge;
† E is the average electric field;
‡ E/N is the average reduced electric field.

Compared to the DBD using the un-frosted quartz tube, the current intensity of the DBD using the frosted tube or the ZrO_2 coated frosted tube is higher, as shown in Fig. 11(a). To get further insights into the characteristics of the discharge, the Lissajous figures of the DBD using different dielectric surfaces were compared (Fig. 11(b)). Table 3 exhibits the specific discharge parameters, calculated from the analyses of the Lissajous figures with the method described previously. [38-40] Under the same conditions, the peak-to-peak charge increases when using the frosted dielectric surface or ZrO_2 coating. The calculated effective capacitance follows the order: ZrO_2 coated surface > frosted surface > un-frosted surface.

The frosted dielectric surface enhances the charge deposition and the formation of local charge accumulation centers on the surface. Moreover, a higher dielectric constant can lead to stronger polarization of dielectric material and higher capacitance [53]. And when the ZrO_2 coated tube is used as the dielectric barrier, the mean electric field is increased by about 18% compared with the un-frosted tube, which results in more micro-discharges. Therefore, the

conversion and energy efficiency of CO_2 decomposition can be significantly improved in this configuration. It is noteworthy that the maximum applied voltage decreases from 13.4 kV of the un-frosted dielectric surface to 12.2 kV with the ZrO_2 coated surface. Considering that the discharge power is the same in each case, the current in the discharge must be increased when using a ZrO_2 coated dielectric surface or frosted dielectric surface, which can also be confirmed from the current signals (Fig. 11a).

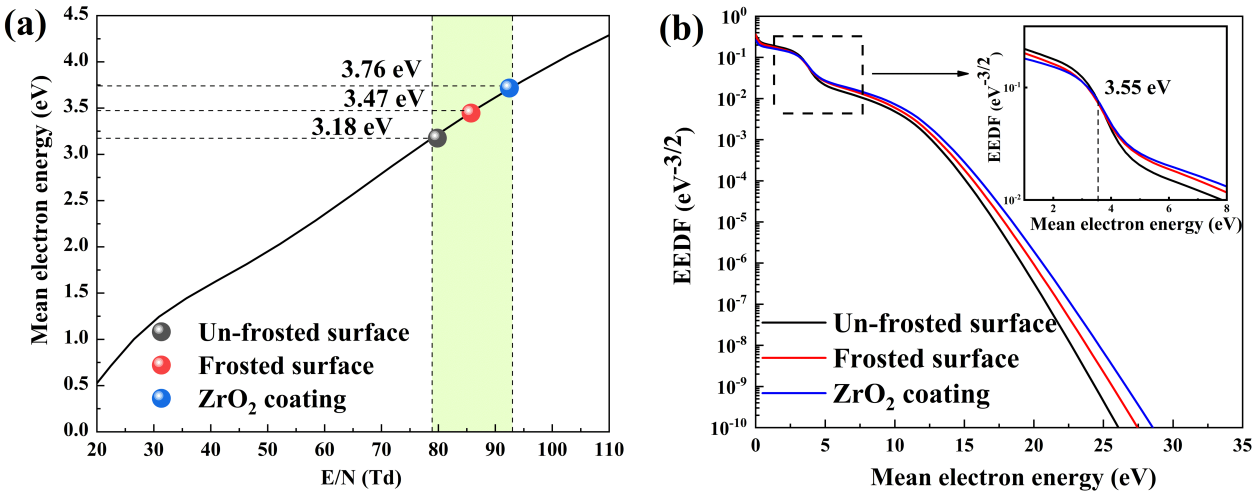

Fig. 12. (a) Calculated mean electron energy as a function of the reduced electric field. (b) Calculated EEDF for three types of dielectric barriers.

The mean electron energy and the electron energy distribution function (EEDF) were calculated with the Boltzmann equation by Boltzmann solver BOLSIG+ [41]. As shown in Fig. 12(a), for the pure CO_2 conversion, the mean electron energy increases with the increase of E/N in DBD. And the colored rectangle shows the range of the average reduced electric field in this study. The order of mean electron energy is: ZrO_2 coated surface (3.76 eV) > frosted surface (3.47 eV) > un-frosted surface (3.18 eV). In addition, the electron energy distribution also

follows this order (Fig. 12(b)). Especially above 3.55 eV, the discharge region with the ZrO_2 coated dielectric barrier generates more energetic electrons.

4. Conclusion

The present work has demonstrated that using the frosted dielectric surface in a DBD reactor significantly improves the energy efficiency and the conversion of CO_2 in the plasma decomposition of CO_2. The ZrO_2 coating on the frosted dielectric surface further improves the energy efficiency and the conversion of CO_2. Compared to the conventional DBD reactor using an un-frosted dielectric surface (e.g., quartz tube), coating ZrO_2 onto the frosted dielectric surface increases the dielectric capacitance, discharge channels and mean electron energy, which further boosts the conversion and the energy efficiency of CO_2 decomposition. This work represents a significant advance in the design of efficient DBD reactors for the conversion of CO_2. To understand the intrinsic characteristic of the DBD plasma decomposition of CO_2, co-reactant such as argon, helium, hydrogen or others, was not employed here. With the use of co-reactant, the energy efficiency and the CO_2 conversion can be further increased, which will be investigated in our future works. The present design of the DBD reactor has a clear advantage in the enhanced micro-discharge performances with negligible influence on the space gas residence time and discharge gap. It is convenient for the preparation of the frosted surface and oxide coating, which can lead to more applications beyond the plasma CO_2 conversion.

Author contribution statement

Chang-jun Liu: Conceptualization, Funding acquisition, Writing-review & editing, Supervision, Project administration. **Xin Tu:** Supervision, Writing-review & editing, Project administration. **Wanyan Ding:** Writing-Original Draft, Validation, Data Curation, Formal

analysis, Investigation. **Mengyu Xia:** Validation, Formal analysis, Data Curation. **Chenyang Shen:** Resources, Methodology. **Yaolin Wang:** Formal analysis, Data Curation. **Zhitao Zhang:** Methodology, Formal analysis, Resources.

Declaration of Competing Interest

The authors declare that they have no known competing financial interests or personal relationships that could have appeared to influence the work reported in this paper.

Acknowledgement

This work was supported by the National Natural Science Foundation of China (No. 22138009). Y. Wang and X. Tu acknowledge the support from the Engineering and Physical Sciences Research Council (No. EP/V036696/1) and the British Council Newton Fund Institutional Links Programme (No. 623389161).

References

[1] J.C. Abanades, E.S. Rubin, M. Mazzotti, H.J. Herzog, On the climate change mitigation potential of CO_2 conversion to fuels, Energy Environ. Sci. 10(12) (2017) 2491-2499. http://dx.doi.org/10.1039/c7ee02819a.

[2] J. Ashok, S. Pati, P. Hongmanorom, Z. Tianxi, C. Junmei, S. Kawi, A review of recent catalyst advances in CO_2 methanation processes, Catal. Today 356 (2020) 471-489. http://dx.doi.org/10.1016/j.cattod.2020.07.023.

[3] S. Liu, L.R. Winter, J.G. Chen, Review of plasma-assisted catalysis for selective generation of oxygenates from CO_2 and CH_4, ACS Catal. 10(4) (2020) 2855-2871. http://dx.doi.org/10.1021/acscatal.9b04811.

[4] D. Mei, X. Tu, Atmospheric pressure non-thermal plasma activation of CO_2 in a packed-bed dielectric barrier discharge reactor, ChemPhysChem 18(22) (2017) 3253-3259. http://dx.doi.org/10.1002/cphc.201700752.

[5] C.J. Liu, G.H. Xu, T.M. Wang, Non-thermal plasma approaches in CO_2 utilization, Fuel Process. Technol. 58(2-3) (1999) 119-134. http://dx.doi.org/10.1016/s0378-3820(98)00091-5.

[6] R. Snoeckx, A. Bogaerts, Plasma technology - a novel solution for CO_2 conversion? Chem. Soc. Rev. 46(19) (2017) 5805-5863. http://dx.doi.org/10.1039/c6cs00066e.

[7] A. George, B. Shen, M. Craven, Y. Wang, D. Kang, C. Wu, X. Tu, A review of non-thermal plasma technology: a novel solution for CO_2 conversion and utilization, Renew. Sust. Energ. Rev. 135 (2021) 109702. http://dx.doi.org/10.1016/j.rser.2020.109702.

[8] H. Puliyalil, D.L. Jurkovic, V.D.B.C. Dasireddy, B. Likozar, A review of plasma-assisted catalytic conversion of gaseous carbon dioxide and methane into value-added platform chemicals and fuels, RSC Adv. 8(48) (2018) 27481-27508. http://dx.doi.org/10.1039/c8ra03146k.

[9] Z. Wang, Y. Zhang, E.C. Neyts, X. Cao, X. Zhang, B.W.L. Jang, C.-j. Liu, Catalyst preparation with plasmas: how does it work? ACS Catal. 8(3) (2018) 2093-2110. http://dx.doi.org/10.1021/acscatal.7b03723.

[10] N. Bouchoul, H. Touati, E. Fourre, J.-M. Clacens, C. Batiot-Dupeyrat, Efficient plasma-catalysis coupling for CH_4 and CO_2 transformation in a fluidized bed reactor: comparison with a fixed bed reactor, Fuel 288 (2021) 119575. http://dx.doi.org/10.1016/j.fuel.2020.119575.

[11] D. Ray, P. Chawdhury, C. Subrahmanyam, A facile method to decompose CO_2 using a g-C_3N_4-assisted DBD plasma reactor, Environ. Res. 183 (2020) 109286. http://dx.doi.org/10.1016/j.envres.2020.109286.

[12] M.R. Jahanbakhsh, H. Taghvaei, O. Khalifeh, M. Ghanbari, M.R. Rahimpour, Low-temperature CO_2 splitting in a noncatalytic dielectric-barrier discharge plasma: effect of operational parameters with a new strategy of experimentation, Energy Fuels 34(11) (2020) 14321-14332. http://dx.doi.org/10.1021/acs.energyfuels.0c02116.

[13] D. Mei, X. Tu, Conversion of CO_2 in a cylindrical dielectric barrier discharge reactor: effects of plasma processing parameters and reactor design, J. CO_2 Util. 19 (2017) 68-78. http://dx.doi.org/10.1016/j.jcou.2017.02.015.

[14] H. Kim, S. Song, C.P. Tom, F. Xie, Carbon dioxide conversion in an atmospheric pressure microwave plasma reactor: improving efficiencies by enhancing afterglow quenching, J. CO_2 Util. 37 (2020) 240-247. http://dx.doi.org/10.1016/j.jcou.2019.12.011.

[15] H.S. Uhm, H.S. Kwak, Y.C. Hong, Carbon dioxide elimination and regeneration of resources in a microwave plasma torch, Environ. Pollut. 211 (2016) 191-197. http://dx.doi.org/10.1016/j.envpol.2015.12.053.

[16] A. Ozkan, T. Dufour, T. Silva, N. Britun, R. Snyders, F. Reniers, A. Bogaerts, DBD in burst mode: solution for more efficient CO_2 conversion?, Plasma Sources Sci. Technol. 25(5) (2016) 055005. http://dx.doi.org/10.1088/0963-0252/25/5/055005.

[17] J. Huang, H. Zhang, Q. Tan, L. Li, R. Xu, Z. Xu, X. Li, Enhanced conversion of CO_2 into O_2-free fuel gas via the Boudouard reaction with biochar in an atmospheric plasmatron, J. CO_2 Util. 45 (2021) 101429. http://dx.doi.org/10.1016/j.jcou.2020.101429.

[18] S. Renninger, M. Lambarth, K.P. Birke, High efficiency CO_2-splitting in atmospheric pressure glow discharge, J. CO_2 Util. 42 (2020) 101322. http://dx.doi.org/10.1016/j.jcou.2020.101322.

[19] N. Britun, T. Godfroid, R. Snyders, Insights into CO_2 conversion in pulsed microwave plasma using optical spectroscopy, J. CO_2 Util. 41 (2020) 101239. http://dx.doi.org/10.1016/j.jcou.2020.101239.

[20] D. Mei, X. Zhu, Y.-L. He, J.D. Yan, X. Tu, Plasma-assisted conversion of CO_2 in a dielectric barrier discharge reactor: understanding the effect of packing materials, Plasma Sources Sci. Technol. 24(1) (2015) 015011. http://dx.doi.org/10.1088/0963-0252/24/1/015011.

[21] V. Vermeiren, A. Bogaerts, Plasma-based CO_2 conversion: to quench or not to quench? J. Phys. Chem. C 124(34) (2020) 18401-18415. http://dx.doi.org/10.1021/acs.jpcc.0c04257.

[22] S. Renninger, P. Rossner, J. Stein, M. Lambarth, K.P. Birke, Towards high efficiency CO_2 utilization by glow discharge plasma, processes 9(11) (2021) 2063. http://dx.doi.org/10.3390/pr9112063.

[23] H. Zhang, L. Li, X. Li, W. Wang, J. Yan, X. Tu, Warm plasma activation of CO_2 in a rotating gliding arc discharge reactor, J. CO_2 Util. 27 (2018) 472-479. http://dx.doi.org/10.1016/j.jcou.2018.08.020.

[24] S.R. Sun, H.X. Wang, D.H. Mei, X. Tu, A. Bogaerts, CO_2 conversion in a gliding arc plasma: performance improvement based on chemical reaction modeling, J. CO_2 Util. 17 (2017) 220-234. http://dx.doi.org/10.1016/j.jcou.2016.12.009.

[25] V. Vermeiren, A. Bogaerts, Improving the energy efficiency of CO_2 conversion in

nonequilibrium plasmas through pulsing, J. Phys. Chem. C 123(29) (2019) 17650-17665. http://dx.doi.org/10.1021/acs.jpcc.9b02362.

[26] N. Lu, C. Zhang, K. Shang, N. Jiang, J. Li, Y. Wu, Dielectric barrier discharge plasma assisted CO_2 conversion: understanding the effects of reactor design and operating parameters, J. Phys. D-Appl. Phys. 52(31) (2019) 319501. http://dx.doi.org/10.1088/1361-6463/ab2171.

[27] S. Zhu, A. Zhou, F. Yu, B. Dai, C. Ma, Enhanced CO_2 decomposition via metallic foamed electrode packed in self-cooling DBD plasma device, Plasma Sci. Technol. 21(8) (2019) 085504. http://dx.doi.org/10.1088/2058-6272/ab15e5.

[28] A. Bogaerts, X. Tu, J.C. Whitehead, G. Centi, L. Lefferts, O. Guaitella, F. Azzolina-Jury, H.-H. Kim, A.B. Murphy, W.F. Schneider, T. Nozaki, J.C. Hicks, A. Rousseau, F. Thevenet, A. Khacef, M. Carreon, The 2020 plasma catalysis roadmap, J. Phys. D-Appl. Phys. 53(44) (2020) 443001. http://dx.doi.org/10.1088/1361-6463/ab9048.

[29] A. Ozkan, T. Dufour, T. Silva, N. Britun, R. Snyders, A. Bogaerts, F. Reniers, The influence of power and frequency on the filamentary behavior of a flowing DBD-application to the splitting of CO_2, Plasma Sources Sci. Technol. 25(2) (2016) 025013. http://dx.doi.org/10.1088/0963-0252/25/2/025013.

[30] S.J. Xu, J.C. Whitehead, P.A. Martin, CO_2 conversion in a non-thermal, barium titanate packed bed plasma reactor: the effect of dilution by Ar and N_2, Chem. Eng. J. 327 (2017) 764-773. http://dx.doi.org/10.1016/j.cej.2017.06.090.

[31] M. Ramakers, I. Michielsen, R. Aerts, V. Meynen, A. Bogaerts, Effect of argon or helium on the CO_2 conversion in a dielectric barrier discharge, Plasma Process. Polym. 12(8)

(2015) 755-763. http://dx.doi.org/10.1002/ppap.201400213.

[32] H. Taghvaei, E. Pirzadeh, M. Jahanbakhsh, O. Khalifeh, M.R. Rahimpour, Polyurethane foam: a novel support for metal oxide packing used in the non-thermal plasma decomposition of CO_2, J. CO_2 Util. 44 (2021) 101398. http://dx.doi.org/10.1016/j.jcou.2020.101398.

[33] D. Ray, P. Chawdhury, K.V.S.S. Bhargavi, S. Thatikonda, N. Lingaiah, C. Subrahmanyam, Ni and Cu oxide supported γ-Al_2O_3 packed DBD plasma reactor for CO_2 activation, J. CO_2 Util. 44 (2021) 101400. http://dx.doi.org/10.1016/j.jcou.2020.101400.

[34] B. Wang, X. Wang, B. Zhang, Dielectric barrier micro-plasma reactor with segmented outer electrode for decomposition of pure CO_2, Front Chem Sci Eng 15(3) (2021) 687-697. http://dx.doi.org/10.1007/s11705-020-1974-1.

[35] G. Niu, Y. Qin, W. Li, Y. Duan, Investigation of CO_2 splitting process under atmospheric pressure using multi-electrode cylindrical DBD plasma reactor, Plasma Chem. Plasma Process. 39(4) (2019) 809-824. http://dx.doi.org/10.1007/s11090-019-09955-y.

[36] R. Valdivia-Barrientos, J. Pacheco-Sotelo, M. Pacheco-Pacheco, J.S. Benitez-Read, R. Lopez-Callejas, Analysis and electrical modelling of a cylindrical DBD configuration at different operating frequencies, Plasma Sources Sci. Technol. 15(2) (2006) 237-245. http://dx.doi.org/10.1088/0963-0252/15/2/008.

[37] S.H. Liu, M. Neiger, Electrical modelling of homogeneous dielectric barrier discharges under an arbitrary excitation voltage, J. Phys. D-Appl. Phys. 36(24) (2003) 3144-3150. http://dx.doi.org/10.1088/0022-3727/36/24/009.

[38] X. Tu, H.J. Gallon, M.V. Twigg, P.A. Gorry, J.C. Whitehead, Dry reforming of methane over a Ni/Al_2O_3 catalyst in a coaxial dielectric barrier discharge reactor, J. Phys. D-Appl. Phys. 44(27) (2011) 274007. http://dx.doi.org/10.1088/0022-3727/44/27/274007.

[39] Y. Uytdenhouwen, S. Van Alphen, I. Michielsen, V. Meynen, P. Cool, A. Bogaerts, A packed-bed DBD micro plasma reactor for CO_2 dissociation: does size matter? Chem. Eng. J. 348 (2018) 557-568. http://dx.doi.org/10.1016/j.cej.2018.04.210.

[40] Y. Wang, M. Craven, X. Yu, J. Ding, P. Bryant, J. Huang, X. Tu, Plasma-enhanced catalytic synthesis of ammonia over a Ni/Al_2O_3 catalyst at near-room temperature: Insights into the importance of the catalyst surface on the reaction mechanism, ACS Catal. 2019, 9, 10780−10793. http://dx.doi.org/ 10.1021/acscatal.9b02538.

[41] G.J.M. Hagelaar, L.C. Pitchford, Solving the Boltzmann equation to obtain electron transport coefficients and rate coefficients for fluid models, Plasma Sources Sci. Technol. 14(4) (2005) 722-733. http://doi.org/10.1088/0963-0252/14/4/011.

[42] I. Michielsen, Y. Uytdenhouwen, J. Pype, B. Michielsen, J. Mertens, F. Reniers, V. Meynen, A. Bogaerts, CO_2 dissociation in a packed bed DBD reactor: first steps towards a better understanding of plasma catalysis, Chem. Eng. J. 326 (2017) 477-488. http://dx.doi.org/10.1016/j.cej.2017.05.177.

[43] E.C. Neyts, A. Bogaerts, Understanding plasma catalysis through modelling and simulation-a review, J. Phys. D-Appl. Phys. 47(22) (2014) 224010. http://dx.doi.org/10.1088/0022-3727/47/22/224010.

[44] A. Ozkan, A. Bogaerts, F. Reniers, Routes to increase the conversion and the energy efficiency in the splitting of CO_2 by a dielectric barrier discharge, J. Phys. D-Appl. Phys. 50(8) (2017) 084004. http:// doi.org/10.1088/1361-6463/aa562c.

[45] P. Chen, J. Shen, T. Ran, T. Yang, Y. Yin, Investigation of operating parameters on CO_2 splitting by dielectric barrier discharge plasma, Plasma Sci. Technol. 19(12) (2017) 125505. http:// doi.org/10.1088/2058-6272/aa8903.

[46] Q. Yu, M. Kong, T. Liu, J. Fei, X. Zheng, Characteristics of the decomposition of CO_2 in a dielectric packed-bed plasma reactor, Plasma Chem. Plasma Process. 32(1) (2012) 153-

163. http://dx.doi.org/10.1007/s11090-011-9335-y.

[47] P. Wu, X. Li, N. Ullah, Z. Li, Synergistic effect of catalyst and plasma on CO_2 decomposition in a dielectric barrier discharge plasma reactor, Mol. Catal. 499 (2021) 111304. http://dx.doi.org/10.1016/j.mcat.2020.111304.

[48] T. Takuma, Field behavior at a triple junction in composite dielectric arrangements, IEEE Trns. Dielectr. Electr. Insul. 26(3) (1991) 500-509. http://dx.doi.org/10.1109/14.85123.

[49] Y.-R. Zhang, E.C. Neyts, A. Bogaerts, Enhancement of plasma generation in catalyst pores with different shapes, Plasma Sources Sci. Technol. 27(5) (2018) 055008. http://dx.doi.org/10.1088/1361-6595/aac0e4.

[50] K. Van Laer, A. Bogaerts, Fluid modelling of a packed bed dielectric barrier discharge plasma reactor, Plasma Sources Sci. Technol. 25(1) (2016) 015002. http://dx.doi.org/10.1088/0963-0252/25/1/015002.

[51] S. Ponduri, M.M. Becker, S. Welzel, M.C.M. van de Sanden, D. Loffhagen, R. Engeln, Fluid modelling of CO_2 dissociation in a dielectric barrier discharge, J. Appl. Phys. 119(9) (2016) 093301. http://dx.doi.org/10.1063/1.4941530.

[52] B. Wang, X. Wang, H. Su, Influence of electrode interval and barrier thickness in the segmented electrode micro-plasma DBD reactor on CO_2 decomposition, Plasma Chem. Plasma Process. 40(5) (2020) 1189-1206. http://dx.doi.org/10.1007/s11090-020-10091-1.

[53] S. Zhang, Z. Chen, B. Zhang, Y. Chen, Numerical investigation on the effects of dielectric barrier on a nanosecond pulsed surface dielectric barrier discharge, Molecules 24(21) (2019) 3933. http://dx.doi.org/10.3390/molecules24213933.